TPM Vol. 32, No. S3, 2025
ISSN: 1972-6325
https://www.tpmap.org/

Open Access

EXPERIMENTAL ANALYSIS OF THE SCOUR EFFECT ON BRIDGE PIERS BY COMPARING SPEEDS AND PRESSURES IN CIRCULAR AND ELLIPTICAL SECTIONS USING AUTODESK CFD

MARIANELLA ISABEL HINOSTROZA MEJIA[1], JESUS EDSGARDO MERINO CARMONA[2], ABEL CARMONA ARTEAGA[3]
[1]BACHELOR OF CIVIL ENGINEERING, LIMA, UNIVERSIDAD PRIVADA DEL NORTE, LIMA, PERÚ
[2]CIVIL ENGINEERING STUDENT, LIMA, UNIVERSIDAD PRIVADA DEL NORTE, LIMA, PERÚ
[3]RESEARCH PROFESSOR, LIMA, UNIVERSIDAD PRIVADA DEL NORTE, LIMA, PERÚ
EMAIL: [1]N00291442@upn.pe [2]N00274918@upn.pe [3]abel.carmon@upn.edu.pe
ORCHID ID:[1] 0009-0002-3948-7234, [2] 0009-0003-0416-6411, [3] 0000-0003-2895-9582

Abstract This research aims to assess the phenomenon of local scour in bridge piers, which is one of the main causes of structural failure, by determining whether there are significant differences in the distribution of hydrodynamic forces and if some bridge pier geometries are more susceptible to scour than others. The research involves the creation of 3D models of a flow table, a circular profile, and an elliptical profile, using Autodesk Inventor Professional software, followed by a simulation that combined numerical calculations and graphical analysis using Autodesk CFD software. In the experimental study, scaled models of circular and elliptical piers were used in a flow table to analyze the drag effect on different profiles. Velocity and pressure measurements were taken to identify critical points prone to scour. The simulation results indicate that the elliptical profile in a 0° orientation shows a significant improvement in reducing both drag and scour in turbulent flows. This study demonstrates the importance of accurately evaluating and controlling the profile orientation, as this can have a substantial impact on the results. This knowledge will enable more informed decisions in the design and the planning of pillars and bridges, as well as the implementation of appropriate protection measures.

Keywords: Autodesk CFD, scour, circular piers, bridges.

INTRODUCTION

The primary objective of a bridge is to connect two communities separated by geography, and the pier plays a crucial role as the column that supports the structure. Additionally, this component transfers the loads to the ground (Jaramillo, 2017).

It is crucial to analyze the behavior of a river around a bridge pier, as turbulent currents and soil scour can occur, potentially leading to instability and structural collapse. For example, the coastal El Niño in Peru affected 180 bridges, 70% of which collapsed due to poor design, as they were not constructed considering the actual river flow and erosion, according to Jorge Abad, director at the Universidad de Ingeniería y Tecnología (Andina agencia peruana de noticias, 2017).

Therefore, it is crucial to thoroughly investigate this effect to understand its implications and develop effective mitigation strategies. Considering the above, comparing velocities and pressures in circular and elliptical sections allows us to examine how the shape of the cross-section influences scour behavior. This research aims to determine whether there are significant differences in the distribution of hydrodynamic forces and if some geometries are more susceptible to scour than others. This knowledge will enable more informed decision-making in the design and planning of piers and bridges, as well as the implementation of appropriate protection measures.

As a reference, we will cite three articles:

In this research, three studies from 2022 and 2023 demonstrated the effectiveness of CFD software in modeling semicircular sections to retain rainwater, achieving results close to real conditions (Janampa-Guardia et al., 2024).

A critical issue in bridge design is local scour, caused by turbulent flows that erode the bed around circular piers due to boundary layer separation, which can lead to structural failures with serious social and economic impacts (Carmona-Arteaga et al., 2022).

Finally, another investigation addressed erosion and overflows generated by heavy rains, simulating barriers in Autodesk CFD to reduce water speed and dissipate energy (Díaz Terrones et al., 2024). These references confirm that simulation tools offer results consistent with reality.

1.1. Autodesk Inventor

The CAD software 3D Inventor provides professional-quality tools for 3D mechanical design, documentation, and product modeling (Autodesk, n.d.).

1.2. Autodesk CFD

The Autodesk CFD software creates computational fluid dynamics models that engineers and analysts use to intelligently predict the behavior of liquids and gases (Autodesk, n.d.).

1.3. Reynolds number in channels

The Reynolds number represents the effects of fluid viscosity in relation to its inertia. It shows that, in open channels, laminar flow occurs when Re < 500. The range of 500 to 2000 is the transition region. Generally, turbulent flow occurs when Re > 2000 (Mott & Untener, 2015).

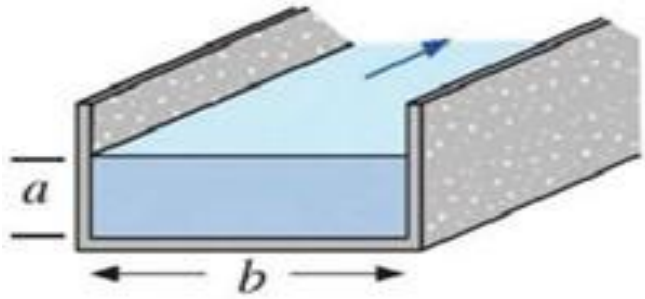

Figure 1 Hydraulic diameter of an open channel (Cengel & Cimbala, 2015).

$$Dh = \frac{4ab}{2a+b} \quad (1)$$

$$Re = \frac{Vprom*Dh*\rho}{\mu} = \frac{Vprom*Dh}{v} \quad (2)$$

Re: Reynolds number
Vprom: average fluid velocity (m/s)
Dh: hydraulic diameter, characteristic length (m)
ρ: fluid density (kg/m³)
μ: Dynamic viscosity of the fluid
v: kinematic viscosity of the fluid (m²/s),

1.4. Drag force

Drag is the force exerted on a body caused by the fluid that resists movement in the direction of the body's displacement. This affects bridge piers by generating lateral forces due to water flow (Mott & Untener, 2015).

1.5. Stagnation point

It is the point on the front surface of an object submerged in a fluid where the fluid velocity decreases to zero. It is the point where the fluid collides with the object and momentarily stops before changing direction and flowing around it (Mott & Untener, 2015).

1.6. Separation or detachment point

It is where the fluid separates from the surface of the body, generating a turbulent wake and reducing pressure. This creates a drag force opposite to the motion (Mott & Untener, 2015).

1.7. Wake

The wake is a turbulence in the fluid flow around a body that results in a decrease in pressure. Pressure drags, also known as form drag, is generated due to this turbulence and is influenced by the shape of the body, the Reynolds number, and the surface roughness (Mott & Untener, 2015). In Figure 2, we can visualize the stagnation point, the separation point and the wake generated by the sphere within the fluid.

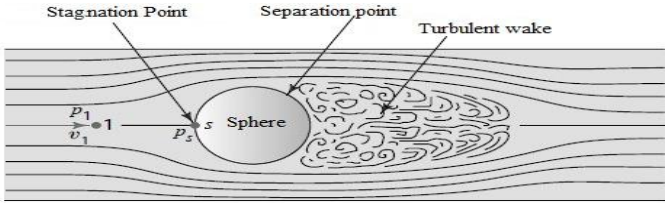

Figure 2 Sphere in a fluid flow showing the stagnation point on the front surface and the turbulent wake behind. (Mott & Untener, 2015).

1.8. Von Karma effect

As the flow approaches the front face of the shedding element, it divides into two streams. The fluid near the body has a lower velocity compared to the speed of the main streamlines. This difference in velocity causes shear layers to form, which eventually break alternately into vortices on both sides of the shedding element. The frequency of the created vortices is directly proportional to the flow velocity and, therefore, to the volume flow rate (Mott & Untener, 2015).

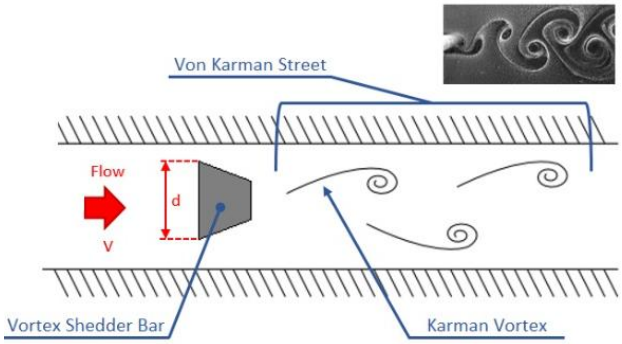

Figure 3 Sketch of the von karman effect (Yokogawa Co-innovating tomorrow, n.d.).

1.9. Iterative method

It is used to solve mathematical problems, such as equations or systems of equations, by using successive approximations to the solution, starting from an initial estimate. This approach differs from direct methods, which attempt to solve the problem in one go (Saad, 20103).

There are numerous interactions that occur in a simulation. At the start of the analysis, the results often vary significantly between iterations, with the convergence lines rising and falling. Once these lines stabilize horizontally, it indicates that the solution has reached convergence and the results no longer change. (Autodesk, n.d.).

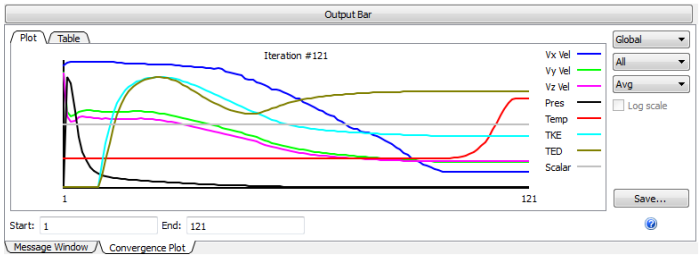

Figure 4 Iterations in Autodesk CFD (Autodesk, 2024.).

1.10. Convergence and divergence of equations

The convergence and divergence of equations refer to the behavior of the solutions of a system of equations as time passes or iterations are performed. Convergence implies that the solutions approach a stable point, while divergence indicates that they move away from or separate from each other(Hirsch, Smale & Devaney, 2017).

Autodesk® CFD continuously monitors variations in the solution field, assessing both local and global fluctuations. When it detects that the solution has converged, meaning the results no longer change, the analysis is automatically stopped before reaching the programmed iterations. This is indicated by a message in the results bar showing the detection of flat lines CFD (Autodesk, 2024.).

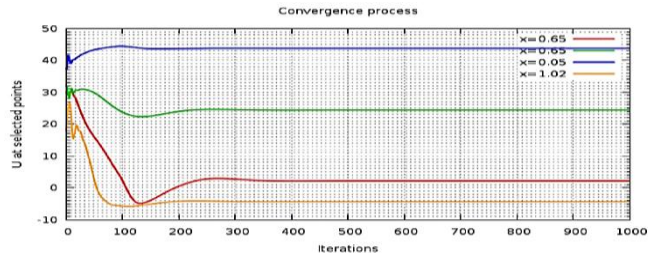

Figure 5 Convergence lines in Autodesk CFD. (Node384, n.d.).

1.11. Navier-Stokes equation

The Navier-Stokes equation is an equation that describes the motion of a viscous fluid, considering factors such as velocity, pressure, and density. It is based on the laws of conservation of mass and momentum. This equation is essential for understanding and predicting fluid behavior in various systems. Autodesk® CFD uses a numerical solution of the Navier-Stokes equations to simulate and analyze fluid behavior in engineering applications (Cengel & Cimbala, 2015).

1.12. Water tables

To calculate the Reynolds number and define the flow state, it is necessary to work with water density (kg/m³) and dynamic viscosity (Pa·s), both in relation to the temperature of the experimental fluid (Mott & Untener, 2015). In our case, we take 22 °C, using an interpolation from Table A.1 in Appendix A of Robert Mott's book for the corresponding temperature.

Table 1 Properties of Water, Appendix A, Table A.1 (p. 488)
Source: Fluid Mechanics - Robert Mott, 7th Edition

Temperature (°C)	Specific Weight (kN/m^2)	Density (kg/m^3)	Dynamic Viscosity (Pa.s)	Kinematic Viscosity (m^2/s)
0	9.81	1000	1.75×10^{-3}	1.75×10^{-6}
5	9.81	1000	1.52×10^{-3}	1.52×10^{-6}
10	9.81	1000	1.30×10^{-3}	1.30×10^{-6}
15	9.81	1000	1.15×10^{-3}	1.15×10^{-6}
20	9.79	998	1.02×10^{-3}	1.02×10^{-6}
25	9.78	997	8.91×10^{-4}	8.94×10^{-7}
30	9.77	996	8.00×10^{-4}	8.03×10^{-7}
35	9.75	994	7.18×10^{-4}	7.22×10^{-7}
40	9.73	992	6.51×10^{-4}	6.56×10^{-7}
45	9.71	990	5.94×10^{-4}	6.00×10^{-7}
50	9.69	988	5.41×10^{-4}	5.48×10^{-7}
55	9.67	986	4.98×10^{-4}	5.05×10^{-7}
60	9.65	984	4.60×10^{-4}	4.67×10^{-7}
65	9.62	981	4.31×10^{-4}	4.39×10^{-7}
70	9.59	978	4.02×10^{-4}	4.11×10^{-7}
75	9.56	975	3.73×10^{-4}	3.83×10^{-7}
80	9.53	971	3.50×10^{-4}	3.60×10^{-7}
85	9.50	968	3.30×10^{-4}	3.41×10^{-7}
90	9.47	965	3.11×10^{-4}	3.22×10^{-7}
95	9.44	962	2.92×10^{-4}	3.04×10^{-7}
100	9.40	958	2.82×10^{-4}	2.94×10^{-7}

1.13. Method for the laminar case

Flows that circulate smoothly and gently are laminar flows, as their movement is slow. The term "laminar" comes from the word "layer," as the flow resembles layers moving together and evenly without mixing with adjacent layers. It is also characterized by a low Reynolds number, typically less than 2000, with the flow exhibiting a uniform diameter (Mott & Untener, 2015).

1.14. CFD Methods for turbulent case

Flows that move quickly, chaotically, and unevenly are called turbulent flows, appearing to be mixed with each other (Mott & Untener, 2015).

1.15. Turbulence models

1.15.1. K-épsilon: It works well for most applications. It is a general purpose turbulence model. Also, it is a default model in the software (Autodesk, 2024).

1.15.2. SST K-Omega: Handles external aerodynamics. SST simulates turbulence up to the wall instead of using wall functions. The mesh must be very fine in the boundary layer region. Handles flows with adverse pressure gradients. Additionally, you can add up to 10 layers using the Wall Layers dialog box (Autodesk, 2024).

1.15.3. SST K-Omega SAS (Scale-adaptive simulation): Flows with transient turbulent structures such as vortex shedding and variable wake structures. You can run steady-state simulations using SST k-omega SAS. While turbulent structures cannot be animated, this model predicts their formation and shape better than a steady-state k-epsilon simulation. Also, the mesh must be very fine in the boundary layer region. You can add up to 10 layers using the Wall Layers dialog box (Autodesk, 2024).

1.15.4. SST K-Omega RC (Smirnov – Menter): High curvature flows, such as those commonly found in cyclonic separators. This is the two-equation Menter model with rotation and curvature correction (RC). It is computationally intensive and requires a fine mesh. Therefore, in some cases, this model may require several thousand iterations for convergence (Autodesk, 2024).

1.15.5. SST K-Omega RC (Hellsten): It works with certain airfoils including the NACA0012 and Coanda airfoils. It also works with small, high-speed rotating devices and highly curved flows over convex surfaces. This is the two-equation Menter SST model with the simplified Hellsten rotation/curvature correction. It shows good prediction of flow over convex surfaces where the separation point can be difficult to predict with other turbulence models (Autodesk, 2024).

1.15.6. SST K-Omega DES (Detached Eddy Simulation): It works with separated external aerodynamic flows and high Reynolds number flows. It is a hybrid between the large eddy simulation (LES) and k-omega SST models. It is a computationally intensive and mesh-sensitive model. It works best with a uniform mesh distribution (Autodesk, 2024).

1.15.7. RNG: Reconnection point for separated flows, particularly for flow over a backward-facing step. More computationally intensive, but sometimes slightly more accurate than the k-epsilon model. It is often recommended to start with the k-epsilon model and switch to RNG after the flow has mostly converged (Autodesk, 2024).

1.15.8. Low Re K-Epsilon: Works with Low velocity turbulent flows, with Reynolds numbers between 1500 and 5000, Flows with high and low velocity regions. Pipe flows and external streamline flows transitioning from laminar to turbulent. High velocity jets entering a large room with slow flow. Buoyancy driven flows (natural convection) that are barely turbulent. This model does not use wall functions. Use at least 5 wall layers. May be less stable than k-epsilon. Requires more iterations to converge compared to k-epsilon. Generally produces the same solution for high velocity flows as k-epsilon. Produces similar results to Laminar selection for laminar flows (Autodesk, 2024).

1.15.9. Mixing length: Works with some internal natural convection analysis. In some cases reduces run times and improves accuracy for buoyancy-driven internal flows. Designed for gas flows (such as air) and does not give good results for liquid flows (Autodesk, 2024).

1.15.10. Eddy viscosity: Works with low velocity turbulent flows and some buoyancy driven flows. It is less rigorous than the k-epsilon model and more numerically stable. Useful if divergence with one of the other models occurs (Autodesk, 2024).

1.16. Computational Fluid Dynamics (CFD)

Computational Fluid Dynamics (CFD) is a branch of fluid mechanics that uses computers to predict flow behavior based on mathematical equations. It is a key tool in design and engineering, applied in areas such as vehicle aerodynamics and cooling systems. CFD is also used in hydraulic engineering to analyze the interaction between fluids and structures, allowing for 2D and 3D visualizations that reduce costs and time in physical experiments. (Carmona, Trigueros & Campos, 2022).

1.17. Saint-Venant equations

The Saint-Venant equations govern the unsteady flow of shallow water in open channels. Derived from the principles of mass and momentum conservation, these equations use differential equations to model variations in discharge and water level over time in a one-dimensional context. They are widely applied in hydraulic engineering to analyze and manage water flow in rivers and channel (Díaz, Cornejo & Carmona, 2024).

1.18. Darcy equation

The Darcy equation describes the flow of fluid through a porous medium, often used in hydrogeology and soil mechanics. It relates the flow rate to the hydraulic gradient and the properties of the porous medium. This equation

indicates that the flow rate is directly proportional to the hydraulic gradient and the area of flow, while being inversely related to the distance over which the head loss occurs (Janampa, Jacinto & Carmona, 2024).

2. METHODS

Flow diagrams were used to represent the steps necessary for creating the parameters utilized in Autodesk Inventor and Autodesk CFD, as shown in Fig 6. They were also used to carry out the corresponding simulations, as presented in Fig 7.

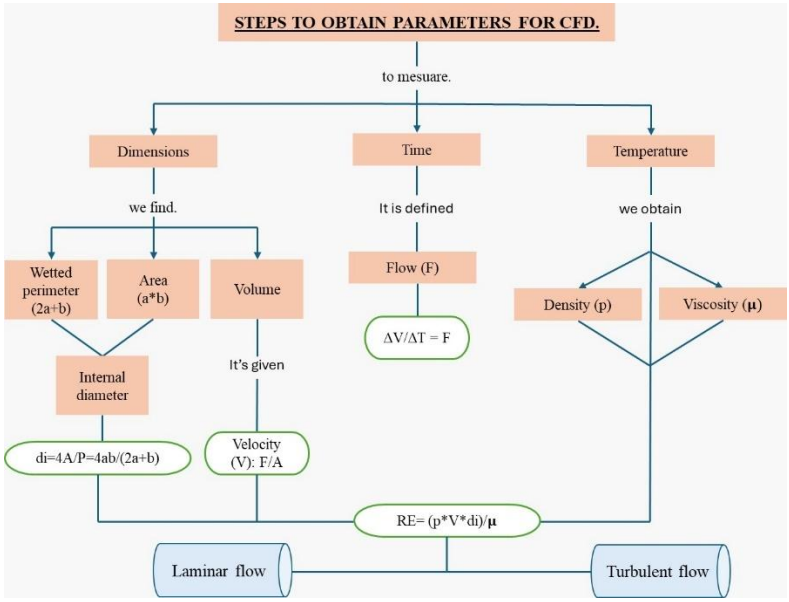

Figure 6 Flowchart of the steps to obtain CFD parameters.

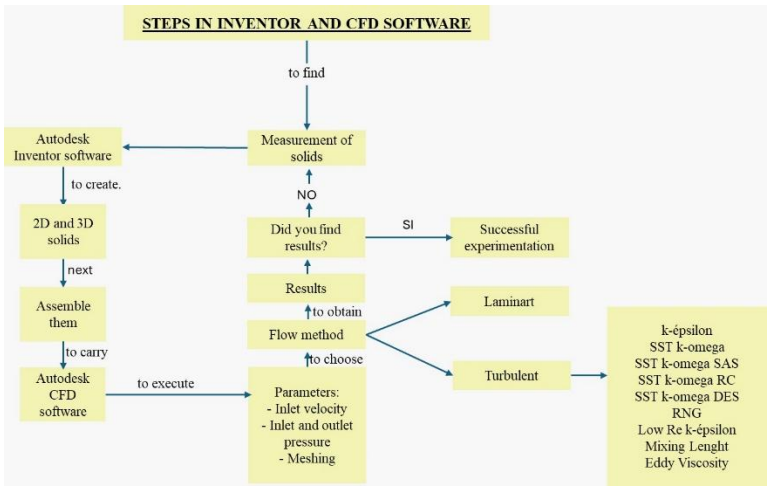

Figure 7 Flowchart of the steps used in Inventor and CFD software.

3. RESULTS AND DISCUSSION

In our research, we worked with both laminar and turbulent flow conditions, focusing on the velocity and pressure of circular and elliptical profiles. Exclusively for the elliptical profile, three different rotation angles were analyzed: 0°, 45° and 90°. The validation of the study was carried out by comparing the results obtained experimentally with those generated through simulations in Autodesk CFD. This analysis allowed us to understand the behavior of the flow under specific conditions, evaluating how the profiles react. The simulations

of laminar and turbulent flows were examined using the velocity parameter. Thus, the velocity planes obtained in the simulations represent their dynamics, allowing the identification of the areas of drag. Similarly, the analysis of the pressure planes facilitated the identification of possible relationships with the scour phenomenon. In Figures 8 and 9, we can observe how the drag wake forms in the circular profile under laminar and turbulent flow, respectively.

Figure 8 Laboratory photograph of drag with laminar flow on a circular profile.

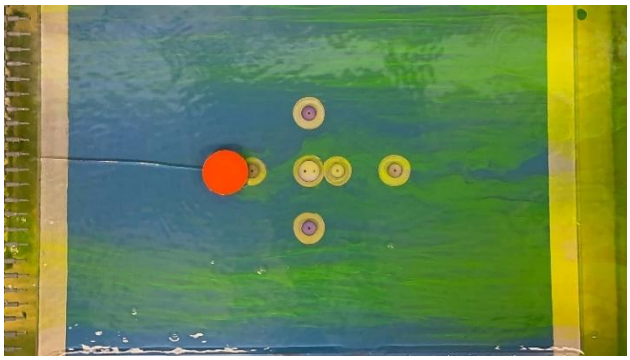

Figure 9 Laboratory photograph of drag with turbulent flow on a circular profile.

In the case of the elliptical profile, three rotation angles were analyzed: 0°, 45° and 90°. Figures 10, 11 and 12 show the drag or wake area produced with this profile at the three angles studied under turbulent flow conditions.

Figure 10 Laboratory photograph of turbulent flow drag in 0° elliptical profile.

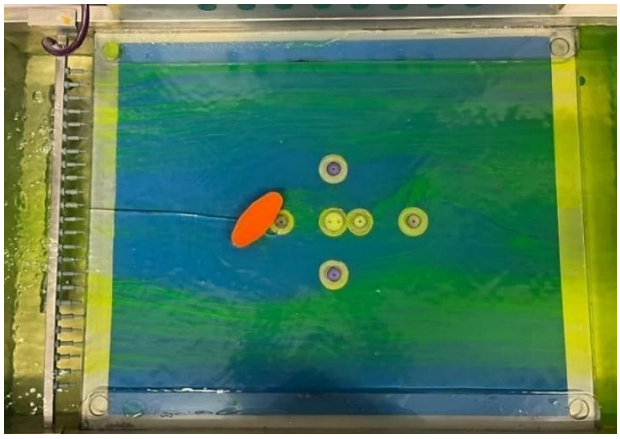

Figure 11 Laboratory photograph of drag with turbulent flow on a 45° rotated elliptical profile.

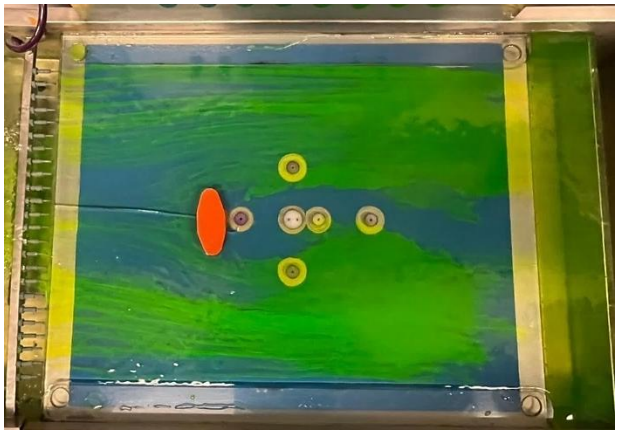

Figure 12 Laboratory photograph of drag with turbulent flow on a 90° rotated elliptical profile.

The dimensions of the container used to calculate the flow rate during the laboratory session were as follows: a width of 0.095 m and a length of 0.6 m, resulting in a total area of 0.057 m². On the other hand, the dimensions of the surface where the profiles were placed were 0.5 m wide and 0.005 m high, giving us a working area of 0.025 m². To determine the inner diameter, the formula indicated in section 1.3 was used, resulting in an inner diameter of 0.019607843 m. By tabulating the measured temperature in the laboratory (22°C) in Table 1, we obtained a water density of 998.20 kg/m³ and a dynamic viscosity of 0.000976 Pa.s.

ESSAY 1

Table 2 Measurements taken during the first laboratory session.

Measures	Height (m)	Time (s)	Volume (m^3)	Caudal (m^3/s)
1	0.01	12.021		
2	0.02	8.092	0.00057	0.00007044
3	0.03	10.023	0.00057	0.00005687
4	0.04	9.089	0.00057	0.00006271
5	0.05	9.067	0.00057	0.00006287
6	0.06	8.067	0.00057	0.00007066
7	0.07	9.079	0.00057	0.00006278
8	0.08	9.046	0.00057	0.00006301
9	0.09	8.066	0.00057	0.00007067
10	0.1	10.006	0.00057	0.00005697
11	0.11	9.052	0.00057	0.00006297
PROMEDIO			**0.00006292**	

The average value obtained from this table gives us the flow rate in cubic meters (m³). Before reaching this point, we previously performed calculations related to the general area data, which now allows us to calculate the velocity by dividing the flow rate by the area. This yields a velocity of 0.025166969 m/s or 2.516696907 cm/s.

Once we have the velocity in meters per second (m/s), we apply the Reynolds formula to determine the type of flow present in the experiment.

$$Re = (v \times L \times \rho)/\mu$$

Using our data with the previous formula, we obtain a Reynolds number of 504.69, which falls within the range corresponding to transitional flow (greater than 500 and less than 4000). However, since it is very close to the lower limit, it will be considered as laminar flow.

ESSAY 2

Table 3 Measurements taken during the second laboratory session..

Measures	Height (m)	Time (s)	Volume (m^3)	Caudal (m^3/s)
1	0.01	1.085	0.00057	0.00052535
2	0.02	2.009	0.00057	0.00028372
3	0.03	2.019	0.00057	0.00028232
4	0.04	3.035	0.00057	0.00018781
5	0.05	1.078	0.00057	0.00052876
6	0.06	2.09	0.00057	0.00027273
7	0.07	2.064	0.00057	0.00027616
8	0.08	2.036	0.00057	0.00027996
9	0.09	2.062	0.00057	0.00027643
10	0.1	2.034	0.00057	0.00028024
	PROMEDIO		**0.00006292**	

Similarly, to the first test, the average value obtained from this table gives us the flow rate in cubic meters (m^3). Before reaching this point, we previously performed the necessary calculations for the general area data, which now allows us to calculate the velocity by dividing the flow rate by the area. Thus, we obtain a velocity value of 0.127738804 m/s or 12.77388044 cm/s. Applying the Reynolds formula again, we obtain a few 2561.6537, which clearly indicates that we are dealing with turbulent flow. Once we have obtained the velocities and identified the types of flow present in each test, we proceed to input these data into the Autodesk CFD software to carry out the corresponding simulation using both the circular and elliptical pillars. Within the CFD software, we proceed to make the necessary configuration: Common setup for both tests: In the materials section, the "ABS model" profile was selected, "glass" was used for the table, and "water" was considered as the fluid. In the boundary conditions, pressures of 10 Pascals were set for the inlet and 0 Pascals for the outlet of the fluid, for both laminar and turbulent flows. In the mesh section, the automatic option was chosen. Specific setup for each test: In the initial conditions, the velocity in cm/s calculated earlier for each flow was entered.

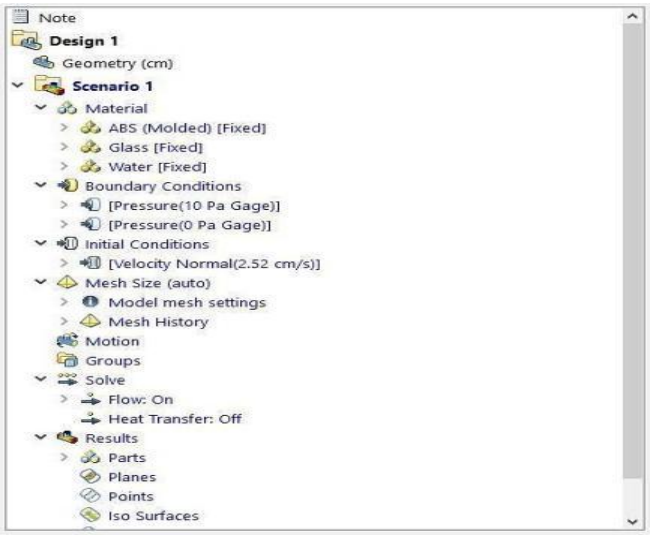

Figure 13 Image of the scenario used in the circular simulation for laminar flow with a velocity of 2.52 cm/s.

Regarding the software used, while modeling both profiles under turbulence, we observed that two of the ten models did not converge correctly: "SST k-omega RC (Smirnov-Menter)" and "SST k-omega RC (Hellsten)." Therefore, they are excluded from this research. On the other hand, the "Eddy Viscosity" model managed to converge, but the simulation results were significantly different from reality, as observed in the laboratory.
Additionally, it is important to highlight that four turbulence models did not perform well in the digital simulation, exhibiting failures in their graphics and showing small white geometric figures without proper representation. These models were "SST k-omega DES (Detached Eddy Simulation)," "RNG," "Low Re k-epsilon," and "Mixing Length." However, we do not rule out the use of these models for future experiments, nor do we claim that they are inefficient; they were simply excluded from this research due to the digital issues.
Two models that succeeded in this research were "k-epsilon" and "SST k-omega," successfully representing digital wakes that closely resembled those observed in the physical experiments conducted in the laboratory. It is important to note that the "SST k-omega SAS (Scale Adaptive Simulation)" model provided a convergence that resembled reality less, as the resulting wake was smaller compared to what was observed in the laboratory.
In Figure 14, the blue wake representing the drag generated by the circular profile in the CFD simulation is shown in detail, working with laminar flow. In this research, not only velocities but also pressures were analyzed.

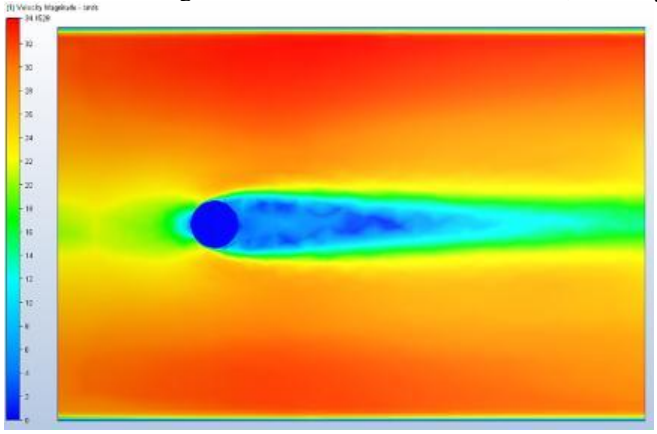

Figure 14 Velocity simulation graph for the circular pillar with laminar flow

In Figure 15, we can clearly observe the pressure zones, where the dark blue area indicates negative pressures, representing areas prone to scouring.

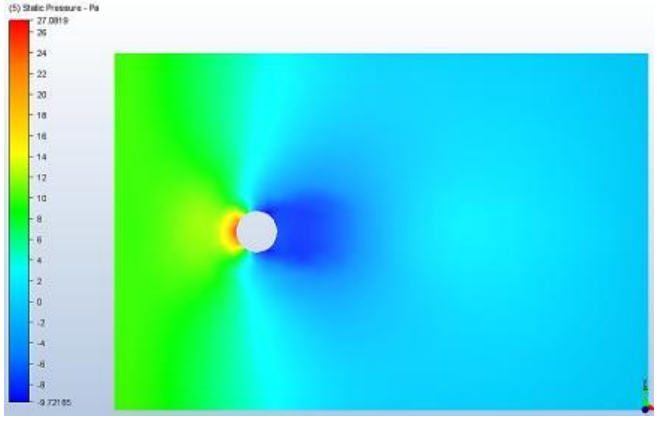

Figure 15 Pressure contour simulation graph for the circular pillar with laminar flow.

In Figure 16, the blue wake can be seen, which represents the drag generated by the circular profile in the CFD simulation. The blue wake also indicates zero velocity, all while working with turbulent flow using the k-epsilon model.

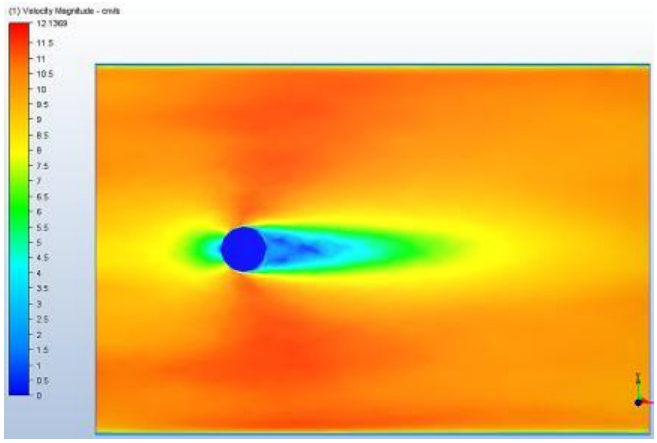

Figure 16 Simulation graph of velocities with turbulent flow using the k-epsilon model of the circular pillar.

In Figure 17 we can clearly see the pressure zones. On the left side of the image, we have a table with numbers and colors that help us identify the areas prone to undermining.

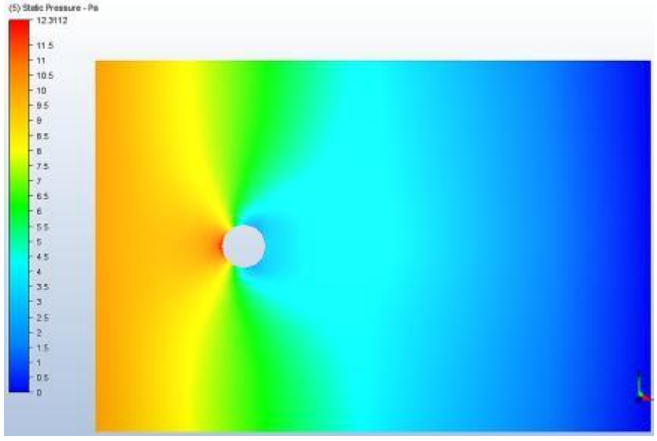

Figure 17 Simulation graph of pressure contours with turbulent flow using the k-epsilon model of the circular pillar.

In Figure 18, it can be seen that the blue wake, which represents the drag generated by the elliptical profile in the CFD simulation, is smaller than that generated by the circular profile, all under laminar flow conditions. It is important to note that the same data was used in both figures for laminar flow. Therefore, we can conclude that the elliptical profile has advantages in terms of reduced drag compared to the circular profile.

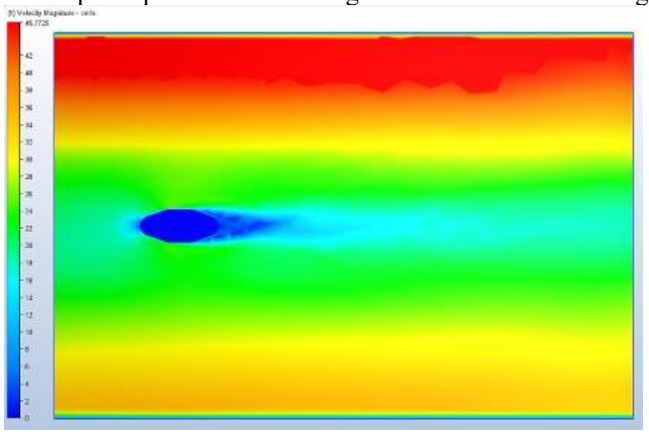

Figure 18 Simulation graph of velocities with laminar flow of the elliptical pillar.

In Figure 19, it can be clearly observed that the pressure zones simulated by the laminar flow with the elliptical profile are lower than the pressures observed in the simulation of the circular profile (Fig. 15). This indicates that the elliptical profile has smaller areas with negative pressures, which in turn translates to a reduction in scour.

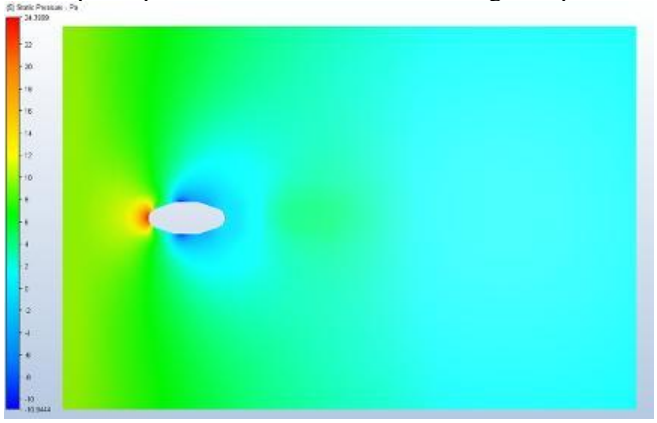

Figure 19 Simulation graph of velocities with laminar flow of the elliptical pillar.

In Figure 20, the very fine blue wake can be observed, which represents the resistance generated by the elliptical profile in the CFD simulation. This was worked with turbulent flow using the k-epsilon model.

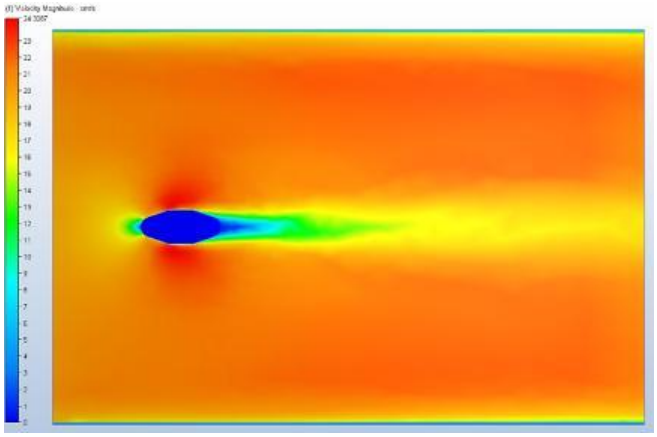

Figure 20 Simulation graph of velocities for the elliptical pillar with turbulent flow using the k-epsilon model.

In Figure 21, we can observe the pressure zones located over the elliptical profile. An important point to note is that, compared to the pressure simulation of the circular profile (Fig. 15), the elliptical profile has a much smaller contact area, meaning a reduced stagnation point. The red color in the figure indicates the stagnation point, where higher pressure is exerted on the elliptical profile in turbulent flow.

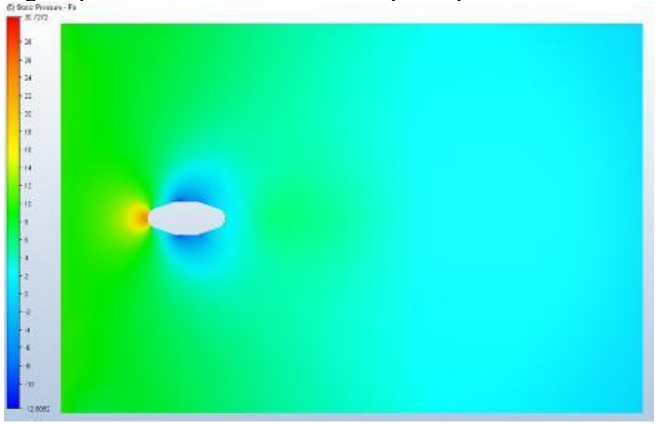

Figure 21 Pressure contour plot of turbulent flow using the k-epsilon model of the elliptical pillar.

Figure 22 shows the CFD simulation generated by the elliptical profile at 0° degrees, which was conducted with turbulent flow using the k-omega SST model. This model allows us to observe a larger blue wake in the simulation,

appearing much wider than the one represented in Figure 20, where the k-epsilon model was used.

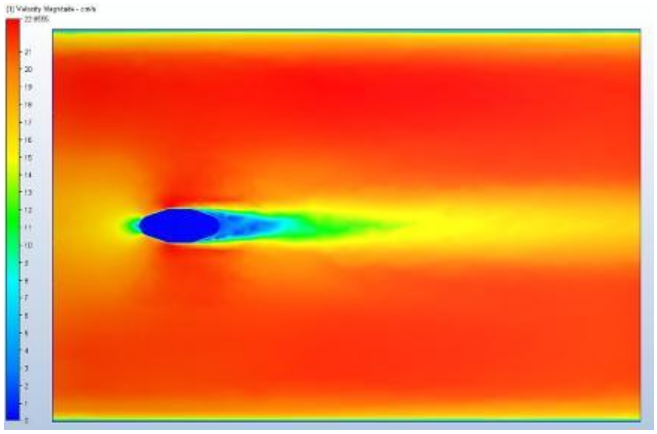

Figure 22 Velocity simulation plot of turbulent flow using the SST k-omega model for the elliptical pillar.

In Figure 23 and 24, velocity and pressure simulations respectively, for a 45° elliptical pillar under a turbulent flow condition using the K-epsilon model, the extension of the wake can be observed as the drag effect experienced by the rotation of the profile. These findings are highly relevant, as they reveal how the orientation of the profile significantly influences its interaction with the flow. When the profile rotates, it generates greater resistance to the flow, which translates into an increase in the drag experienced by the profile. This drags, in turn, contributes to the formation of a wider and more pronounced wake compared to the profile at 0°.

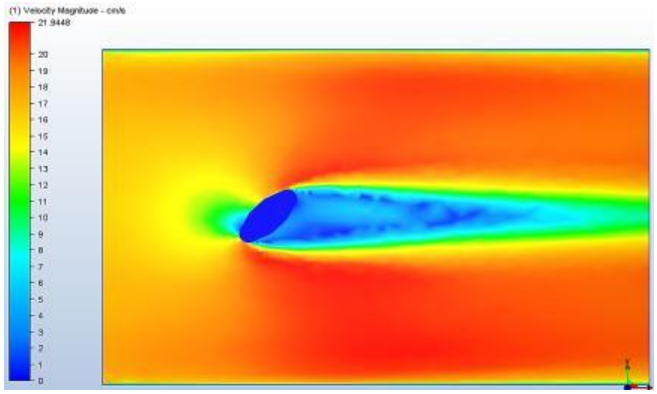

Figure 23 Velocity simulation plot of turbulent flow using the k-epsilon model for the elliptical pillar rotated 45°.

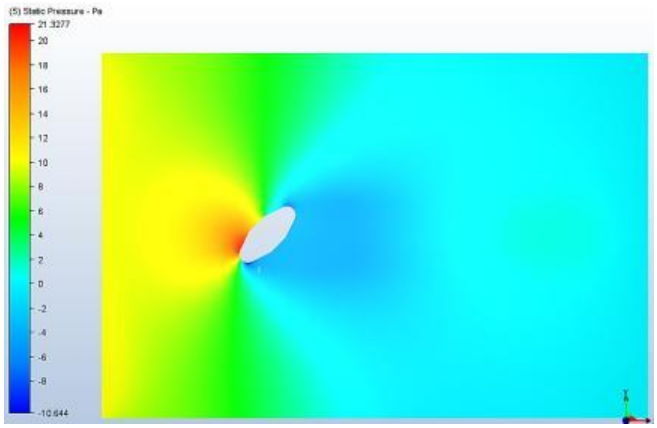

Figure 24 Pressure contour simulation plot of turbulent flow using the k-epsilon model for the elliptical pillar rotated 90°.

Figures 25 and 26 show CFD simulations under turbulent flow conditions using the k-epsilon model and the elliptical profile rotated 90° degrees. This shows us the importance and how much the rotation of a pier can affect bridges.

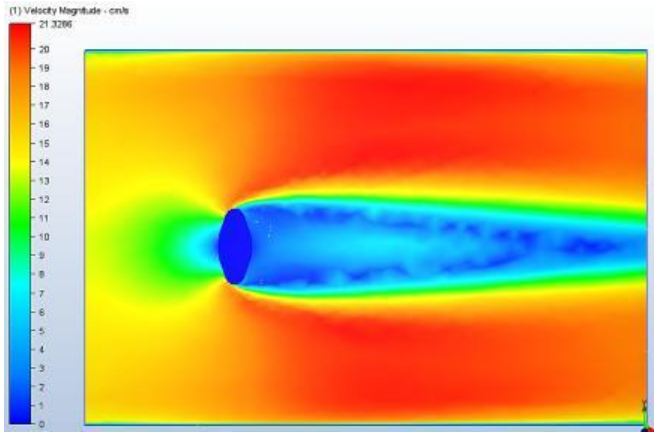

Figure 25 Velocity simulation plot of turbulent flow using the k-epsilon model for the elliptical pillar rotated 90°.

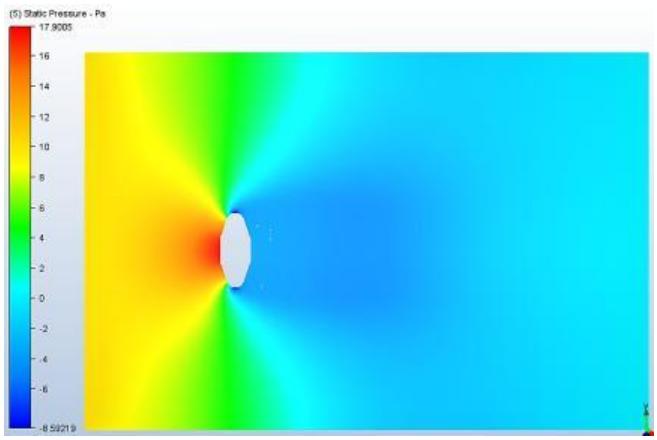

Figure 26 Pressure contour simulation plot of turbulent flow using the k-epsilon model for the elliptical pillar rotated 90°.

4. CONCLUSIONS

After a thorough analysis, it is concluded that the elliptical profile in the 0° orientation is highly effective in reducing drag and scour in turbulent flows, making it a favorable option for bridge pier construction. However, a significant impact is observed when the profile orientation changes, as evidenced in the figures where it is rotated to 45° and 90°, showing a considerable increase in drag and scour. Therefore, it is crucial to carefully consider the profile orientation to achieve optimal performance.

It is recommended to use the elliptical profile for bridge piers after conducting a rigorous analysis and defining a range of river flow directions. In conditions with minimal variation in flow direction, the elliptical profile proves to be highly effective in mitigating drag and scour, providing a solid and reliable solution.

Additionally, the elliptical profile offers the advantage of lacking sharp angles, unlike rectangular or square profiles. This rounded characteristic of the elliptical profile makes it more resistant to structural damage, making it an even safer and more viable option for bridge pier applications.

In conclusion, the analysis of flow dynamics reveals that the increase in fluid velocity has critical implications, especially regarding the negative pressures generated on submerged body profiles. This phenomenon not only leads to the formation of larger scour zones, which pose a significant risk to the integrity of hydraulic structures, but also accelerates structural deterioration.

Moreover, the manifestation of the von Kármán effect in the fluid wake at high velocities introduces additional complexity by making it more difficult to identify areas that require protection. Therefore, it becomes evident that a comprehensive and rigorous approach is necessary in the design and protection of these structures to ensure their sustainability and safety against the challenges posed by fluid dynamics.

Ethical considerations: Not applicable

Conflict of Interest: The authors declare no conflicts of interest.

Funding: This research did not receive any financial support.

REFERENCES

- Jaramillo - Paul JBF (2017) Evaluación del efecto de la geometría de pilares en la socavación del cauce. Tesis, Universidad de Piura.
- Empresa Peruana de Servicios Editoriales S. A. EDITORA PERÚ. (2017). Casi el 70 % de puentes colapsados por lluvias estaba mal diseñado. https://andina.pe/agencia/noticia-casi-70-puentes-colapsados-lluvias-estaba-mal-disenado-664914.aspx Accessed on June 3, 2023.
- Janampa-Guardia, J. I., Jacinto-Ferrer, H. J., & Carmona-Arteaga, A. (2024). Study of semicircular sections through CFD software for rainwater retention in arid areas. En Sustainable Engineering for a Diverse, Equitable, and Inclusive Future at the Service of Education, Research, and Industry for a Society 5.0. Conferencia llevada a cabo en San José, Costa Rica. https://doi.org/10.18687/LACCEI2024.1.1.175
- Carmona-Arteaga, A., Trigueros-Cervantes, G. A., & Campos-Vasquez, N. (2022). Modelación de Dinámica de Fluidos Computacional (CFD) del efecto de socavación local en pilares circulares de puentes. En M. M. Larrondo Petrie, J. Texier, & R. A. R. Matta (Eds.), Proceedings of the 2nd LACCEI International Multiconference on Entrepreneurship, Innovation and Regional Development: Exponential Technologies and Global Challenges: Moving Toward a New Culture of Entrepreneurship and Innovation for Sustainable Development, LEIRD 2022 (Vol. 2022-December). https://doi.org/10.18687/LEIRD2022.1.1.202
- Díaz Terrones, J. L., Cornejo Meléndez, J. A., & Carmona Arteaga, A. (2024). Design of two-dimensional solids for the reduction of velocities and pressures in water resources using CFD and Inventor software. En Sustainable Engineering for a Diverse, Equitable, and Inclusive Future at the Service of Education, Research, and Industry for a Society 5.0. Conferencia llevada a cabo en Costa Rica. https://doi.org/10.18687/LACCEI2024.1.1.116
- Autodesk. (n.d.). Autodesk Inventor: software de modelado 3D para diseñadores e ingenieros. Autodesk https://www.autodesk.com/latam/products/inventor/overview?term=1-YEAR&tab=subscription&plc=INVPROSA . Accessed on June 3, 2023.
- Autodesk. (n.d.). Autodesk CFD: Simulation software for engineering complex liquid, gas, and air systems. Autodesk. https://www.autodesk.com/products/cfd/overview?term=1-YEAR&tab=subscription&plc=SCFDM Accessed on June 3, 2023.
- Mott, R., & Untener, J. (2015). Mecánica de fluidos (7ª ed.). Addison Wesley (pp. 375-488).
- Yokogawa co-innovating tomorrow. (n.d.). Yokogawa: Medidores de flujo. Yokogawa https://www.yokogawa.com/mx/solutions/products-and-services/measurement/field-instruments-products/flow-meters/vortex-flow-meters/#Descripci%C3%B3n-General . Accessed on June 3, 2023.
- Saad, Y. (2003). Iterative methods for sparse linear systems (2a ed.). SIAM (pp. 103–128).
- Autodesk. (n.d.). Autodesk CFD 2024: Chapter 12: Can I Trust my Results?. Autodesk CFD 2024 https://help.autodesk.com/view/SCDSE/2024/ENU/?guid=GUID-9D30EB08-3C45-419B-BEC6-976606AC46F5 Accessed on June 3, 2023.
- Hirsch, M., Smale, S., & Devaney, R. (2017). Differential equations, dynamical systems, and an introduction to chaos (3a ed.). Academic Press (pp. 329-359).
- Autodesk. (2024). Autodesk CFD 2024. https://help.autodesk.com/view/SCDSE/2024/FRA/?guid=GUID-E9E8ACA1-8D49-4A49-8A35-52DB1A2C3E5F Accessed on June 3, 2023.
- Node384 - CFD SUPPORT. (n.d.). Notes on Convergence. CFD SUPPORT. https://www.cfdsupport.com/openfoam-training-by-cfd-support/node384.html
- Cengel, Y., & Cimbala, J. (2015). Mecánica de fluidos: fundamentos y aplicaciones (2ª ed.). McGraw-Hill (pp. 11-593).